Meteorologische Zeitschrift, Vol. 27, No. 5, 401–415 (published online September 28, 2018)
© 2018 The authors

Evaluation of a Wind Farm Parametrization for Mesoscale Atmospheric Flow Models with Aircraft Measurements

Simon K. Siedersleben[1]*, Andreas Platis[2], Julie K. Lundquist[3,4], Astrid Lampert[5], Konrad Bärfuss[5], Beatriz Cañadillas[6], Bughsin Djath[7], Johannes Schulz-Stellenfleth[7], Jens Bange[2], Thomas Neumann[6] and Stefan Emeis[1]

[1]Institute for Meteorology and Climate Research (IMK-IFU), Garmisch-Partenkirchen
[2]Environmental Physics, ZAG, University of Tübingen
[3]University of Colorado, Department of Atmospheric and Oceanic Sciences, Boulder, Colorado
[4]National Renewable Energy Laboratory, Golden, Colorado
[5]Institute of Flight Guidance, Technische Universität Braunschweig
[6]UL–DEWI GmbH
[7]Institute for Coastal Research, Helmholtz Zentrum Geesthacht

(Manuscript received December 15, 2017; in revised form July 25, 2018; accepted September 14, 2018)

Abstract

Large offshore wind farms are usually clustered around transmission grids to minimize the expense of transmission, due to military zones, pipelines, and due to other uses such as nature preserves. However, this close proximity can undermine power production in downwind wind farms due to wakes from upwind wind farms. Therefore, the wind energy industry has great interest in determining the spatial dimensions of offshore wind farm wakes to assess the economical potential of planned wind farms. In this work we use wake measurements conducted by a research aircraft to evaluate the performance of a wind farm parameterization (WFP) in a mesoscale model during stably-stratified atmospheric conditions, in which the wake is expected to be the strongest. The observations were conducted on the 10 September 2016 within the project WIPAFF (Wind PArk Far Field) at the North Sea. The observations allow evaluation of both the horizontal and the vertical dimensions of the wake. The model simulates the length and most of the time the spatial dimensions of the wake. Further, we show that the largest potential for improving the performance of the WFP is rooted in an improvement of the background flow. This is due to the fact that the mesoscale model has problems representing the atmospheric boundary layer in the transition between land to open sea.

Keywords: wind farm parametrization, airborne measurements, marine atmospheric boundary layer, offshore wind farm, wind farm wake

1 Introduction

Offshore wind energy plays a major role in the renewable energy industry. According to WindEurope (2016), the offshore market experienced the largest investments within the wind energy sector in the year 2015. These large investments are motivated by stronger and steadier wind speeds in addition to less turbulent conditions compared to onshore sites (Bilgili et al., 2011).

Although the wind resources offshore are considerable, evidence suggests that wind turbine wakes can also undermine those resources. Due to stably-stratified atmospheres over the sea during spring (Dörenkämper et al., 2015), wakes of large offshore wind farms can exceed 20 km (Christiansen and Hasager, 2005; Djath et al., 2018). Simplified analytic models (e.g. Frandsen et al., 2006; Emeis, 2010) have proposed such long wakes. Hasager et al. (2015) confirmed these results using satellite synthetic aperture radar data to estimate wind speed downwind of offshore wind farms. They observed wakes with extents up to 70 km.

As connections to transmission grids are expensive, offshore wind farms are clustered, frequently with separation less than 10 km. For example, the wind farms Amrumbank West and Nordsee Ost/Meerwind SuedOst in the North Sea are only 5 km apart (see Figure 1). Hence, a wake produced by an upwind located wind farm causes an economic loss for a wind farm located further downwind (e.g. Kaffine and Worley, 2010; Nygaard, 2014; Nygaard and Hansen, 2016; Bodini et al., 2017). Furthermore, wakes of wind farms also influence the stratification of the atmosphere. For example, Baidya Roy and Traiteur (2010), Zhou et al. (2012) and Fitch et al. (2013a) showed that a single onshore wind farm can impact surface temperatures by nearly 1°C. Especially during nocturnal stable conditions, a warming of the atmosphere in the lower rotor area can occur (Fitch et al., 2013a) by mixing warmer air towards the surface.

Motivated by these questions, several numerical simulations were conducted in the past on different scales.

*Corresponding author: Simon Siedersleben, Institute for Meteorology and Climate Research (IMK-IFU), Kreuzeckbahnstr. 19, 82467 Garmisch-Partenkirchen, Germany, e-mail: simon.siedersleben@kit.edu

DOI 10.1127/metz/2018/0900
© 2018 The authors

Large-eddy simulations were used to investigate the flow properties within wind farms (e.g. Calaf et al., 2010; Calaf et al., 2011; Porté-Agel et al., 2011; Wu and Porté-Agel, 2015; Vanderwende et al., 2016) and to gain insight in wakes of single wind turbines (Chatelain et al., 2013). Compared to LES, mesoscale models are computational inexpensive and can therefore cover an area with several thousand square kilometers like the German Bight. Consequently, mesoscale simulations are suitable tools to estimate the wind energy resources at offshore sites (Hahmann et al., 2015). However, the grid size of mesoscale simulations is too large to simulate the effects of single wind turbines explicitly, hence wind farm parameterizations are used to estimate the effect of wind farms on the *far-field* [1]. In the past wind farms in mesoscale and global models were represented as an area with increased surface roughness length as it was done by Ivanova and Nadyozhina (2000) and Keith et al. (2004). However, this surface-roughness-based approach leads to an exaggerated warming over the wind farm and an underestimation of wind speed deficits during night time (Fitch et al., 2013b).

Recently, two wind farm parameterizations for mesoscale numerical models were introduced by Fitch et al. (2012) and Volker et al. (2015). Both studies represent wind turbines as an elevated momentum sink, but the impact of the wind turbines on the turbulent kinetic energy (TKE) is captured differently. Fitch et al. (2012) adds TKE at rotor height, depending on the thrust and power coefficient whereas other wind farm parameterizations (e.g. Jacobson and Archer, 2012; Volker et al., 2015) let the TKE evolve from the field rather than adding it directly. The wind farm parameterization of Abkar and Porté-Agel (2015) is based like the one of Fitch et al. (2012) on the theory of Blahak et al. (2010). The major difference between the wake farm parameterization of Fitch et al. (2012) and Abkar and Porté-Agel (2015) is the fact that the wind farm parameterization of Abkar and Porté-Agel (2015) accounts for the wind farm layout by introducing a parameter ξ. This parameter ξ can be used to tune the parameterization for un- and staggered wind farms. However, this parameter has to be obtained from large-eddy simulations (Abkar and Porté-Agel, 2015).

Although mesoscale modelling studies (e.g. Fitch et al., 2012; Volker et al., 2015) suggest wakes longer than 40 km, only few studies have focused on evaluating these wind farm parametrizations. Volker et al. (2015) used two mast measurements to verify the simulated wind deficit of Horns Rev, 2 km and 6 km downwind of the wind farm under neutral conditions. They found a difference between model and observation smaller than 0.15 m s^{-1}. An error of the same order was found for the averaged wind speed within the wind park at hub height, by implementing the wind farm parametrization of Fitch et al. (2012) into the regional climate model (COSMO-CLM) and comparing it against large-eddy simulations (Chatterjee et al., 2016). Jiménez et al. (2015) used turbine specific thrust and power curves and could improve the power prediction. Lee and Lundquist (2017) evaluated the wind farm parameterization of Fitch et al. (2012) with wind turbine power production data and showed that the parameterization significantly improved the power forecast compared to a control simulation without the parameterization.

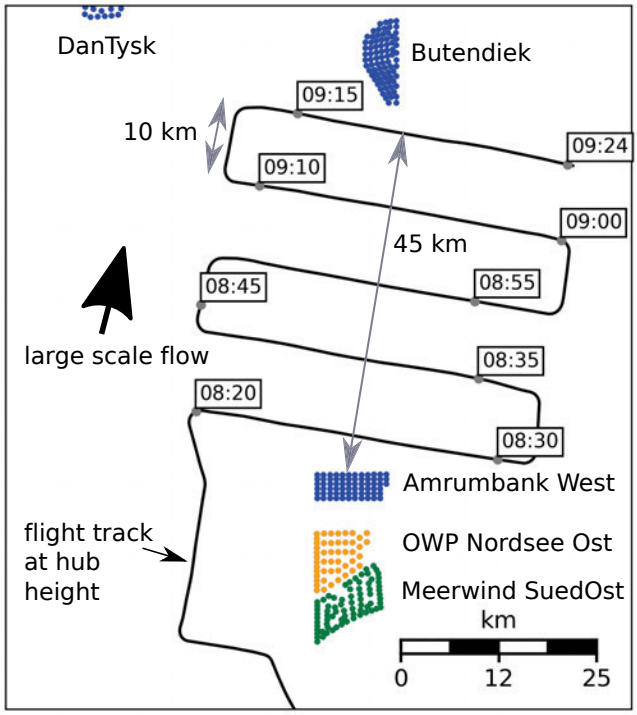

Figure 1: The wind farms of interest, the flight track of the research aircraft with time stamps in UTC and the mean wind direction during the field campaign on 10 September 2016. The black box in Figure 2b indicates the location of the shown close-up. Every single wind turbine is plotted as a dot and the corresponding wind farms Meerwind SuedOst (MSO, green dots), OWP Nordsee Ost (NO, orange dots), Amrumbank West (AW), Butendiek and DanTysk are annotated in the Figure. The flight track is indicated with a black solid line. The orientation of the wind direction is denoted by an arrow.

However, all these studies – except the works of Lee and Lundquist (2017) and Hasager et al. (2015) – evaluated mesoscale wind farm parameterization under *idealized* conditions. More specifically, they used neutrally stratified atmospheres, stationary inflows and neglected moisture effects in their simulations. However, offshore wind farms located close to the coast are exposed to stably stratified atmospheres, especially during spring and early summer (e.g. Smedman et al., 1996; Smedman et al., 1997; Dörenkämper et al., 2015). In addition to that, coastal topography highly influences the offshore wind field (Dörenkämper et al., 2015). Therefore, there is the need to test the performance of wind farm parameterizations for offshore real case simulations.

[1] By far-field we refer throughout the whole manuscript to the area 5 km and more downwind of a wind farm.

An evaluation of a parameterization for a real case simulation faces an extra challenge. It is compared to idealized simulations necessary to evaluate the deviation of the background flow with respect to the observations. Otherwise it is not clear whether a deviation between simulation and measurements is rooted in the background flow or in the parameterization itself. As we evaluate in this study a wind farm parameterization we have special interest in the ability of the mesoscale model to simulate the upwind wind speed profile that is in turn strongly dependent on the correct representation of the atmospheric stability.

In this study we evaluate the wind farm parameterization of Fitch et al. (2012) by the use of airborne in-situ data. These airborne measurements of wakes at the North Sea were executed within the German Research project WIPAFF (Emeis et al., 2016). We focus in this work on a wake that was observed downwind of the three wind farms Meerwind SuedOst (MSO), Nordsee-Ost (NO) and Amrumbank West (AW) on 10 September 2016. The location of the wind farms of interest is shown in Figure 1 and 2. During the campaign, winds were southerly as indicated in Figure 1. Wakes were observed as far as 45 km north of these farms (Platis et al., 2018). The simulations were conducted with the *Weather Research & Forecasting Model* (WRF) (Skamarock et al., 2008) in combination with the wind farm parameterization of Fitch et al. (2012). We try to answer the following questions in this work.

- Is the WRF model able to simulate the upwind flow?
- How well does the parameterization of Fitch et al. (2012) resolve the spatial extent of wakes generated by large offshore wind farms?
- Is the deviation induced by the wind farm parameterization negligible compared to the background error?

In Section 2, we present the numerical setup for our simulation and the aircraft measurements. An overview about the synoptic conditions during the field campaign is given in Section 3. The Section control run contains two Sections. We first evaluate the model upwind of the wind farms in Section 4.1 and 4.2 before we move on to the evaluation of the simulated wakes in Section 4.3. To account for uncertainties in the simulations we present a sensitivity study in Section 5. This is followed by a discussion of the results (Section 6) and a conclusion (Section 7).

2 Dataset and method

2.1 Ground-based observations

We use ECMWF analysis data to assess the weather on a synoptic scale for this case study. The vertical structure of the atmosphere upwind of the wind farms is captured by the sounding of the island Norderney (Figure 2), which is available at 0000 UTC (i.e., 8 hours before the aircraft measurements commenced).

Below 60 m mean sea level (MSL), no flight measurements were possible, therefore we use the observations of the measurement towers FINO1 and FINO3 to assess the lower marine atmosphere, up- and downwind of the wind farms of interest (location of towers is shown in Figure 2). In contrast to the sounding of Norderney, FINO1 and FINO3 have the advantage that they are not influenced by the land surface and, hence, give representative stratification of the marine boundary layer below hub height. Moreover, FINO3 was not influenced by any wakes. In contrast, FINO1 was likely influenced by Borkum Riffgrund 1. Therefore, the temperature and wind measurements at FINO1 have to be used with caution. FINO1 is equipped with five temperatures sensors at 33 m, 50 m, 70 m, 90 m and 100 m above MSL, whereas FINO3 has only 3 temperature sensors at 50 m, 70 m, and at 90 m above MSL (Neumann et al., 2004). The temperature sensors at FINO1 have an absolute accuracy of 0.5 K (Fruehmann, 2018, personal communication) and agree relative to each other with an accuracy of ±0.05 K (Fruehmann, 2016). The temperature sensors at FINO3 have an absolute uncertainty of 1.21 K (Mark, 2018, personal communication).

2.2 Airborne observation

The aircraft Dornier 128-6, operated by the TU Braunschweig, observed wind speed, humidity, temperature and pressure at a sampling frequency of 100 Hz. These measurements are a key feature of this work, as they capture the spatial extent of wakes. The flight measurements took place on the 10 September 2016 from 0800 UTC to 1100 UTC.

The research aircraft flew two different flight patterns to capture the vertical and horizontal extent of the wake. The horizontal flight pattern is shown in Figure 1 with flight legs perpendicular to the mean wind speed. The first flight leg was flown 5 km downwind of the wind farm. Four further flight legs 15 km, 25 km, 35 km and 45 km downwind of the wind farms were also flown (see Platis et al., 2018 for more details).

The vertical extent of the wake 5 km downwind of the wind farms was observed by 5 flight legs at 5 different heights: 60 m, 90 m, 120 m, 150 m and 220 m above MSL. The vertical flight pattern took place from 1000 UTC to 1100 UTC.

To be aware of the upwind flow conditions and to provide a sound basis for the model evaluation, the aircraft probed the atmosphere upwind of the wind farms of interest at 0800 UTC. The location of the climb flight is shown in Figure 2. These vertical profiles are presented in Section 3.2 and are compared to the simulations in Section 4.1.

The aircraft measurements have two kinds of errors – a systematic and a relative error. The systematic error is rooted in the accuracy of the sensor itself. The temperature sensor has an accuracy of 0.2 K (Corsmeier et al., 2001), and the wind speed measurements an accuracy of 0.5 m s^{-1} with a resolution of 0.08 m s^{-1} (Brümmer et al., 2003). The relative error is rooted in the size

of the eddies of the atmosphere and, hence, the measurement strategy, as the error is a direct function of the sampling length (Mann and Lenschow, 1994). The airborne measurements are area-averaged over 300 and 3000 data points for the climb flight and for the horizontal flight pattern, respectively. By averaging over different length scales we systemically under- or overestimate the turbulent values and standard deviations of temperature and wind speed. Following Mann and Lenschow (1994), we have a relative error of 10 % during the climb flight and 1 % during the horizontal flight pattern for the wind speed measurements (Platis et al., 2018). The temperature observations have a relative error of 0.015 K during the climb flight. As we use area averages in our data analysis to investigate the spatial variation of temperature and wind measurement, the relative error is applicable. The corresponding Gaussian error propagation for the wind direction is ±3°.

2.3 Numerical setup and ECMWF analysis data

All simulations are conducted with the Weather Research & Forecasting Model WRF, version 3.8.1 (ARW, Skamarock et al., 2008). The model uses three domains with a horizontal grid size of 15 km, 5 km and 1.6 km, respectively. The location of the two way nested domains is shown in Figure 2. The time step is 60 s for the coarsest domain, 20 s and 5 s for the following domains, respectively. The initial and lateral boundary conditions are defined with operational ECMWF analysis data in 6 hourly intervals and a grid size 0.125 degrees. Simulations with ERA-INTERIM reanalyses data were performed as well, but the wind direction and the stratification of the atmosphere were better represented with the ECMWF analysis data. The sea surface temperature (SST) affects the stratification of the atmosphere, hence, mesoscale simulations with refined SST (such as that provided via the Operational Sea Surface Temperature and Sea Ice Analysis (OSTIA) product), can improve mesoscale simulations (Shimada et al., 2015). However, the SST data from OSTIA for this case only differs marginally from the SST data provided from ECMWF analysis data. Therefore, we did not update the SST using an advanced SST dataset. Hahmann et al. (2015) pointed out that boundary layer winds over land have a spin-up time larger than 12 hours and could therefore influence offshore boundary layer wind climatology. Therefore, our model is initialized at 1200 UTC 9 September 2016 and integrated over 24 hours (i.e., to have a spin-up of more than 12 hours, the observation started at 0800 UTC).

A high number of vertical levels within the rotor area seems important to resolve the effect of the wind farms as precisely as possible. In idealized simulations the number of vertical levels within the rotor area had only a minor effect on the extent of wakes (Fitch et al., 2012). In comparison with large-eddy simulations, increased vertical resolution did not offer consistent improvements in simulating mesoscale wakes (Vanderwende et al., 2016). However, significant improvement was achieved by Lee and Lundquist (2017) by using three and six vertical levels below and within the rotor area, instead of one level and four levels, respectively. Nevertheless, in this study we obtained results closest to the observation with one full level below the rotor area and only three levels within the rotor area. This vertical resolution is equal to a vertical spacing of 35 m in the lowest 200 m and increasing to 100 m at 1000 m above MSL. The model top is at 100 hPa (i.e., 15 km above MSL).

The wind farm parameterization of Fitch et al. (2012) is used to capture the effect of wind farms on the boundary layer. This parameterization is by default implemented in the WRF-ARW since version 3.3 (Skamarock et al., 2008). This wind farm parameterization acts as an elevated sink for the mean flow and as a source of turbulence, depending on the thrust and on the power coefficient. The power coefficient (c_p) describes the fraction of energy that is converted from kinetic energy into electrical energy, whereas the thrust coefficient (c_t) is the total fraction of energy that is extracted from the atmosphere. The difference between c_p and c_t is caused by mechanical, electrical and nonproductive drag. The mechanically and electrically induced losses are neglected in the parameterization of Fitch et al. (2012). Consequently, nonproductive drag on its own explains then the difference between c_p and c_t. By assuming that all nonproductive drag produces turbulence, $c_t - c_p$ describes the fraction of kinetic energy that is converted into turbulent kinetic energy (TKE). A comprehensive description of this parameterization is found in Fitch et al. (2012).

The following parameterizations are used in all three domains: the WRF double-moment 6-class cloud microphysics scheme (WDMS; Lim and Hong, 2010), the Rapid Radiative Transfer Model for GCM (RRTMG) scheme for short- and longwave radiation (Iacono et al., 2008), the Noah land surface model (Chen and Dudhia, 2001) and the Mellor-Yamada-Nakanishi-Niino (MYNN) boundary layer parameterization (Nakanishi and Niino, 2004). In the two innermost domains convection is resolved explicitly, only the first domain uses the cumulus parameterization of (Kain, 2004).

2.4 Wind farms implemented in the numerical simulation

Six different wind farms are implemented in the model: Butendiek, DanTysk, Godewind 1 and 2, Amrumbank West (AW), Meerwind SuedOst (MSO) and Nordsee Ost (NO). All these wind farms are shown in Figure 1, except Godewind 1 and 2. The locations of the wind farms Godewind 1 and 2 can be seen in Figure 6. The focus is on the wake that was generated by the wind farms AW, MSO and NO. The wind farms Butendiek, DanTysk, Godewind 1 and 2 were parmeterized to see any wake interactions and influence on the upwind flow of AW, MSO and NO. In these six different wind farms,

three different wind turbine types are installed. The different turbine types in the wind farms are summarized in Table 1.

Every wind turbine type has its unique power and thrust coefficient depending on the wind speed. However, these coefficients are rarely accessible to the public. Therefore, we used the coefficients of the the wind turbine type Siemens SWT 3.6-120-onshore as these are available online (see, http://www.wind-turbine-models.com/turbines/646-siemens-swt-3.6-120-onshore, accessed October 9, 2018). This is of course a potential source of error (Fitch, 2015). Consequently, these coefficients have to be used with care: According to one-dimensional flow theory, thrust and power coefficients are independent of the rotor size. Therefore, we use the same coefficients for all three wind turbine types. However, the rotor diameter and the nominal power were adapted in the corresponding WRF configuration tables.

To estimate the magnitude of this source of error, sensitivity studies with altered thrust coefficients were conducted. The sensitivity experiments are presented in Section 5 and are discussed in Section 6.

3 Observation

First, an overview of the meteorological conditions prior to and during the field experiment is given in Section 3.1, followed by Section 3.2, where we examine the vertical structure of the atmosphere. Due to advection of warm air over the cold water surface from the nearby land surface, the atmosphere at the wind farms was stably-stratified.

3.1 Synoptic and mesoscale overview

A trough centred over the Faroe Islands at 0600 UTC 10 September 2016 (i.e., 2 hours before the research flight started) was associated with a southwesterly flow at the German Bight and a cold front at 925 hPa, extending from south England to the southern end of Norway (Figure 3a). The front was orientated parallel to the mean flow and was therefore almost stationary and did consequently not directly influence the German Bight. The southwesterly flow caused warm air advection over the North Sea at 925 hPa (Figure 3b).

The flow upwind of the wind farms of interest was highly influenced by the land surface. From 0600 UTC to 1200 UTC the wind direction changed from southwesterly to southerly. As the wind rotated, the distance from the wind farms to the coast decreased. Therefore, the rapidly-warming land surface exerted a stronger influence on the boundary layer upwind of the wind farms. Especially, in the second half of the field experiment, warm air was advected from the warmer land surface - the northern part of Germany. This pattern typically causes a stably-stratified atmosphere over the Baltic Sea (e.g. Dörenkämper et al., 2015; Svensson et al., 2016) and is therefore also relevant for the North Sea. Therefore, we investigate the vertical stratification of the atmosphere in detail in the following section.

3.2 Vertical structure of the atmosphere

According to analytical models, the vertical and lateral transport of momentum determines the wake recovery (Emeis, 2010). The vertical transport of momentum is in turn heavily influenced by the stratification of the atmosphere. Therefore, we assess in this section the vertical state of the atmosphere during the field experiment.

Stable conditions occurred between 60 m and 100 m above MSL in the ascent portion of the flight leg, as seen in the potential temperature profiles (Figure 4). Above 100 m, a strong inversion (i.e. 0.02 K m^{-1}) extends to rotor-top (150 m). Above the rotor area the atmosphere is still stably stratified but with a weaker vertical positive potential temperature gradient (i.e. 0.003 K m^{-1}) than within the rotor area.

Further upwind of the ascent flight, at FINO1, the atmosphere was more weaker stratified below 40 m MSL at 0800 UTC. Figure 5 shows the vertical temperature profile of FINO1 and FINO3 at 0800 UTC, 0900 UTC and 1000 UTC. The SST at FINO1 was 292.5 K at 0800 UTC whereas the air temperature at 40 m was 292.2 K. When the measurement uncertainties are considered, these measurements suggest that the atmosphere was either slightly stably stratified or neutrally stratified below 40 m.

It is most likely that the weakly stratified layer was caused by cold air advection stemming from the nocturnal inversion of the land surface located approximately 100 km upwind, as indicated by the sounding of Norderney that was taken at 10 September 00 UTC (i.e. 8 hours before the climb flight). The potential temperature profile of the sounding matches the one taken by the aircraft. This emphasizes that the nocturnal inversion of the land surface was advected by the large scale southerly flow. However, the absence of a weakly stratified layer in the sounding indicates that the ocean warmed the lower atmosphere over the ocean and destabilized the lower atmosphere at FINO1.

From 0900 UTC onward, warm air advection dominated the stratification of the atmosphere upwind of the wind farms. Therefore, the weakly stratified layer below 40 m experienced a stabilization at FINO1. For example, at 1000 UTC a SST of 292.7 K was observed at FINO1 and 292.7 K at 40 m, indicating a stably stratified layer in the lowest 40 m of the atmosphere.

In contrast, at FINO3 the lower atmosphere was stably-stratified during the whole measurement campaign. This was mainly caused by a colder SST further away from the coast (Figure 3) and the fact that FINO3 was not affected by the cold air advection of the nocturnal inversion. This is evident from Figure 5, over the whole observational period the SST was colder than the lowest air temperature measured at FINO3 at 23 m MSL. Consequently, the lower atmosphere was stably stratified at FINO3.

Over the course of the day, the air above land warmed faster than the marine boundary layer. This warm air reached the marine boundary layer close to the coast

Table 1: Wind turbine types installed in the model according to the data of the Bundesnetzagentur (2017).

wind farm	wind turbine type	hub height (m)	diameter (m)
DanTysk	SIEMENS SWT 3.6-120	90	120
Butendiek	SIEMENS SWT 3.6-120	90	120
Godewind	SIEMENS SWT-6.0-154	110	154
Amrumbank West	SIEMENS SWT 3.6-120	90	120
Meerwind SuedOst	SIEMENS SWT 3.6-120	90	120
OWP Nordsee Ost	SENVION 6.2	95.4–97.04	126

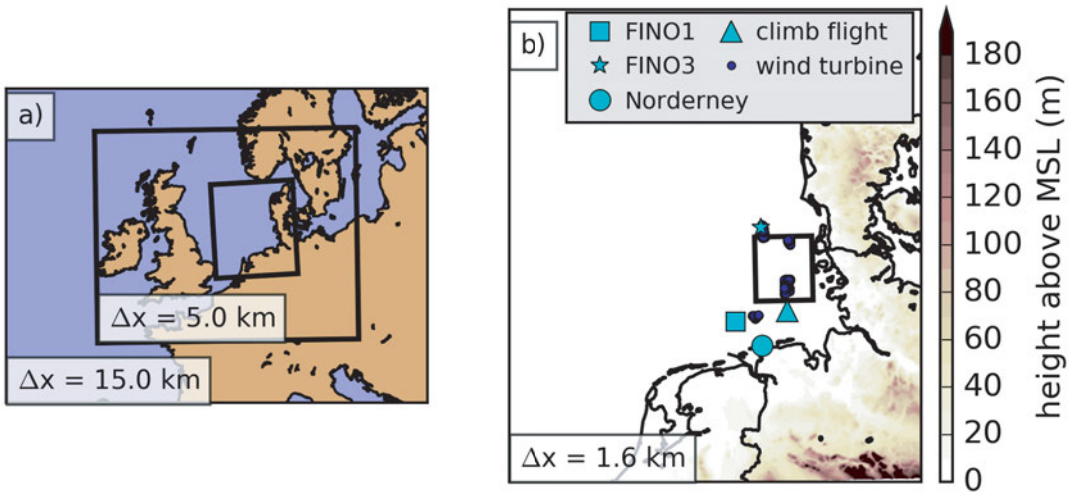

Figure 2: WRF model domains and a close up on the innermost model domain: (a) locations of the three model domains with a grid size of 15, 5 and 1.6 km, respectively. The innermost domain of (a) is shown in detail in (b). Color contours show the topography, dark blue dots represent the locations of single wind turbines and appear as blue area due to the high density of wind turbines. The black box in (b) denotes the location of the close-up shown in Figure 1.

around 0900 UTC (Figure 5b), therefore the lower boundary layer at FINO1 became also stable.

The stably-stratified atmosphere, 60 m above MSL, was associated with a weak low-level jet between 100–300 m (Figure 4). Below hub height, the wind speed varied between 6 m s^{-1} and 7 m s^{-1}; above hub height, the wind speed increased up to 7.3 m s^{-1} at 150 m above MSL, the height of the top of the inversion. At 250 m MSL the wind speed decreased to 5 m s^{-1}.

4 Control run

In this section the results of the control run (i.e. simulation with wind farms) are presented. We first verify the upwind flow to provide a sound basis for the error discussion of the wind farm parameterization presented in Section 6. We further compare then the wake measurements with our simulations.

4.1 Verification of the background flow

As described in Section 2.2, the research aircraft probed the atmosphere approximately 20 km upwind of the wind farms (Figure 3b). The measured wind speed and potential temperature are shown in Figure 4a) and b), respectively. To evaluate the upwind flow, we interpolated the WRF data spatially onto the track of the climb flight of the research aircraft. Every blue dot in Figure 4 represents the value of a single vertical level.

Figure 4b) reveals that WRF captures the inversion at the rotor area height but has a bias of approximately 1 K up to a height of 400 m. Above 400 m, the model represents the atmosphere well. Below hub height, the model shows a neutrally-stratified layer, which could not be evaluated by aircraft measurements as the aircraft was not allowed to fly below 60 m MSL. However, the contrast between SST and the lower atmosphere influences the marine boundary layer (Friehe et al., 1991). Therefore, we use data from FINO1 and FINO3 to evaluate the marine boundary layer close to the surface (Figure 5).

Figure 5 reveals the same problem as the flight measurements, an offset of approximately 1 K close to the surface during the whole flight campaign at 0800 UTC and at 0900 UTC. Nevertheless, one hour later at 1000 UTC, the lower marine boundary layer warmed faster than in the simulation (Figure 5c). Measurements at FINO1 Figure 5c) show an almost isothermal atmosphere with a temperature equal to the SST, whereas the model has a negative vertical temperature gradient with a temperature colder than the SST. Consequently, the model was not as stably stratified as reality at 1000 UTC.

With increasing fetch from the coast, the model performance improves. Vertical temperature profiles of

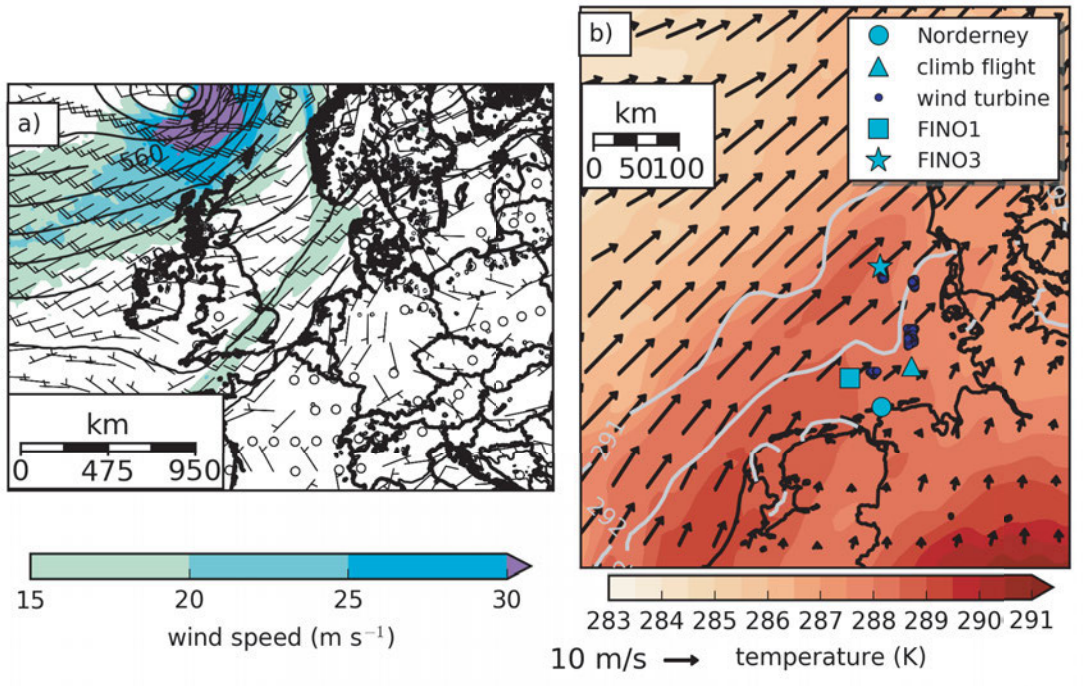

Figure 3: ECMWF analysis at 0600 UTC 10 September 2016: (a) 925-hPa analysis of geopotential height as black contour lines (40 m increment), wind barbs (half and full barbs for 2.5 m s^{-1} and 5 m s^{-1}, respectively, circles denote wind speeds below 2.5 m s^{-1}) for the horizontal wind field. (b) The 925-hPa analysis of potential temperature as colored contours (0.5-K increment).

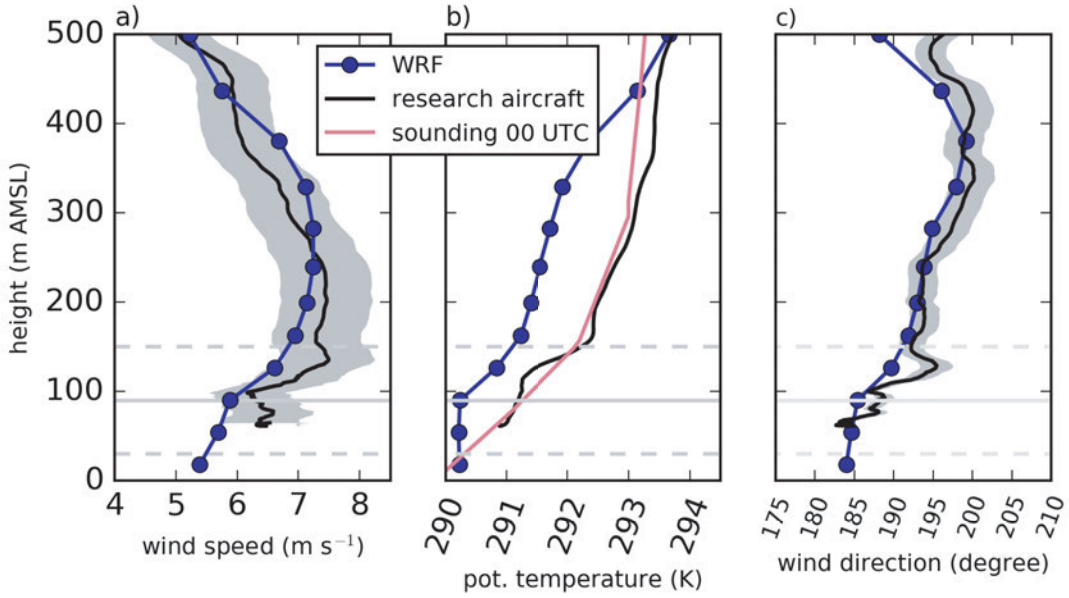

Figure 4: Vertical profiles of (a) wind speed, (b) potential temperature and (c) wind direction measured by the aircraft at the location indicated in Figure 3. The simulation results were spatially interpolated onto the flight track and are plotted in blue colors. Every blue dot denotes a full WRF level. The sounding for Norderney at 0000 UTC 10 September 2016 is indicated by a red line. Grey shadings indicate the relative errors of the measurements. The climb flight and sounding location are shown in Figure 2 and Figure 3. The rotor area of the turbines is marked with dashed grey lines and the hub height (90 m above MSL) with a grey solid line.

FINO3 and WRF match, especially at 0800 UTC and 0900 UTC. At 1000 UTC the simulation is 0.2 K warmer than FINO3.

Wind speed measurements agree well with the model results (Figure 4), showing an increase in wind speed up to a height of 250 m MSL. However, within the rotor area, the model underestimates the wind speed by up to 1.0 m s^{-1}. Above the rotor area, simulation and observation agree well. Above 250 m, the model overestimates the wind speed by 1 m s^{-1}, corresponding to a

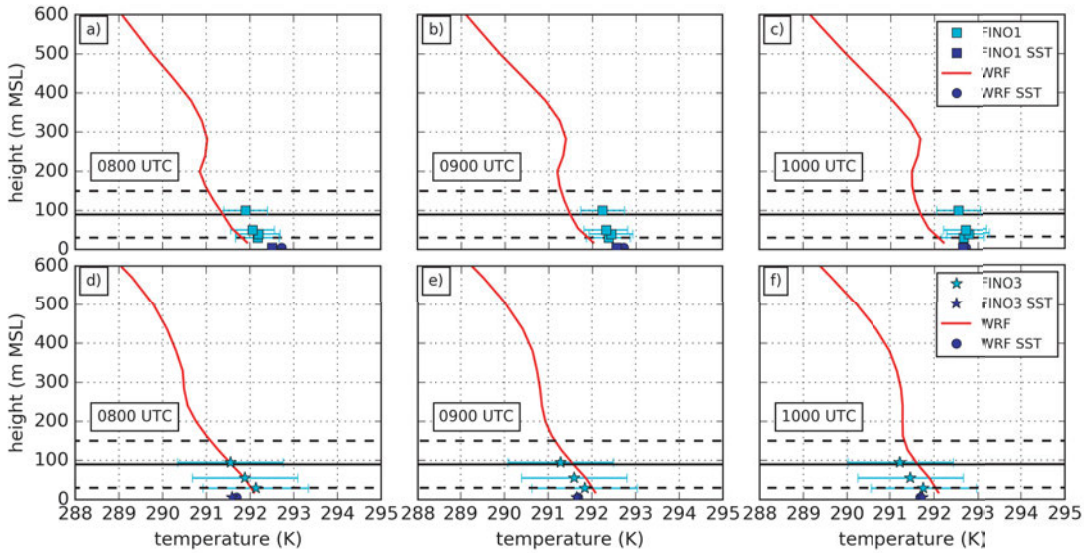

Figure 5: Evaluation of the stratification up- and downwind of the wind farms at FINO1 (top three panels) and FINO3 (bottom three panels) at 0800 UTC, 0900 UTC and 1000 UTC 10 September 2016. The location of these measurement towers are indicated in Figure 3. The simulated profiles are plotted in red. The rotor area and hub height are indicated as in Figure 4.

more pronounced inversion in the model compared to the observations. Above 400 m, model and observation agree within 0.5 m s^{-1}.

The model simulates the wind directions well. However, during the second half of the measurement flight, the mean flow shows more southerly flow than the simulations (discussed later).

4.2 Evolution of the wind field upwind of the wind farms

The simulated horizontal wind field at hub height (Figure 6) shows higher wind fields over the open ocean than over land, due to lower surface friction over the ocean and the incoming trough (Figure 3a) approaching the German Bight from the north-west.

Near to the coast of the German Bight, streaks of reduced wind speeds can be observed as in Dörenkämper et al. (2015). In their study, these streaks are caused by the varying surface roughness at the coast line. Consequently, the wind field upwind of the wind farms is not homogeneous in space.

Further, the wind speed in the observational area decreased during the flight campaign, as seen in Figure 7a–c) and from the measurements at FINO1 (not shown). Upwind of the wind farms, the simulated wind speed decreases from 6.0–6.5 m s^{-1} down to 5.5–6.0 m s^{-1}. This decrease is likely due to the sea breeze circulation aligned with the large scale flow in the morning hours opposite to the large-scale flow as soon the adjacent land warmed. Consequently, the wind farms AW, MSO and NO experienced lower upwind wind speeds at the end of the flight campaign.

In summary, the wind field was inhomogeneous in time and space. In order to compare the model output to the observations at nearly-simultaneous times,

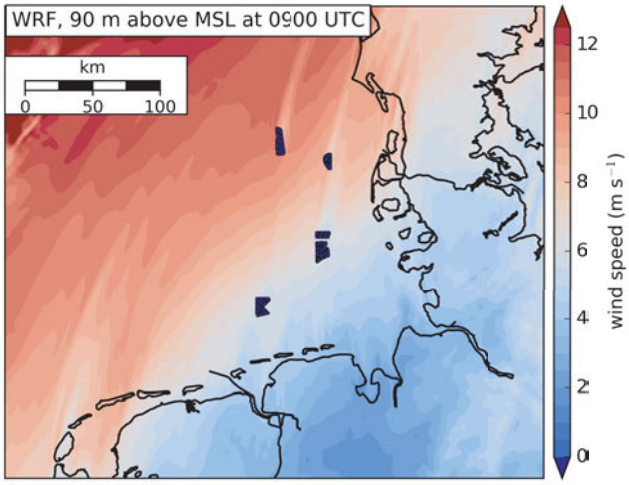

Figure 6: Coastal effects on the wind field 90 m above MSL at 0900 UTC, 10 September 2016. The horizontal wind speed is shown with colored contours. The location of the wind turbines are marked with blue dots. A more detailed look on the wind turbine distribution within the wind farms Meerwind SuedOst, NordseeOst and Amrumbank West is provided in Figure 1.

we use model output that was averaged over all simulated time steps (available for every 5 minute interval) from the time period over which the data collection occurred. For example, the first flight leg collected data from 0820–0830 UTC. Therefore, in Figure 7e), the WRF simulations for the first leg consider only WRF model output averaged from 0820–0830 UTC. The second flight leg consists of data collected from 0835–0845 UTC, and so the model data pictured in Figure 7e). Panel f) is simply the difference between the data visualized in d and e. The results of this method are presented in detail in the following section.

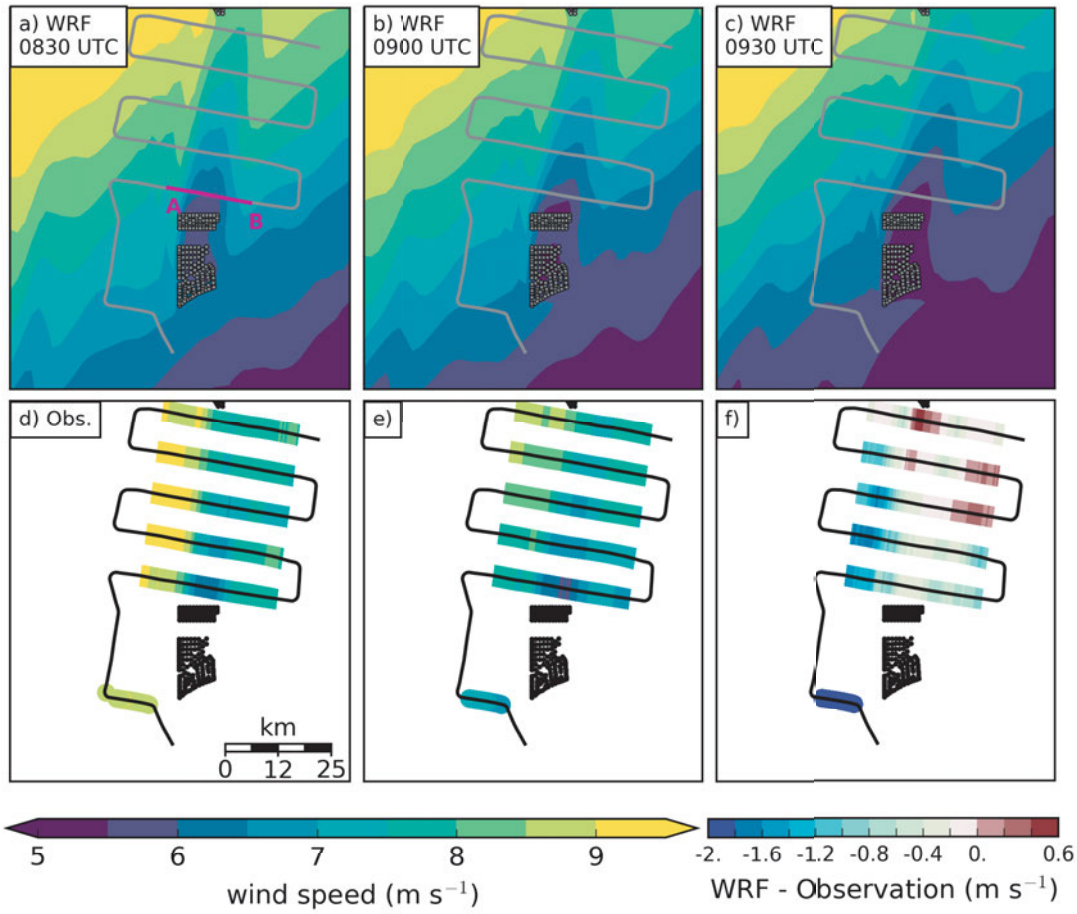

Figure 7: Comparison of simulated and measured wind speed at hub height in the far field of the wind farm. The simulated wind speed at hub height during the observational period (a) 0830, (b) 0900 and (c) 0930 UTC is shown in colored contours. The observed wind speed at hub height is shown in (d) in the same colored contours as the simulation results (e). The black line denotes the flight track. Black dots indicate the locations of the single wind turbines. In (e) the simulation results were interpolated onto the flight track, spatially and timely, for details – see text. In (f) the difference, WRF (e) – observation (d) along the fight track is plotted. The vertical cross section shown in Figure 8 is shown by a pink line, with the beginning and end of cross section annotated with A and B, respectively.

4.3 Wake simulations

4.3.1 Horizontal extent of the wake

The spatial dimensions of the modeled and observed wakes agree well. Figure 7 compares the observed and the simulated wake that was obtained with the wind farm parametrization of Fitch et al. (2012). We show the simulated wind speed at hub height at 0830 UTC, 0900 UTC and 0930 UTC in Figure 7a–c) to suggest the development of the wake and the upwind conditions. The observed wake is shown in Figure 7d), the simulated wind speed interpolated onto the flight track in Figure 7e) and the deviation between WRF and observation, in Figure 7f).

Both the model and the observation show a wake extending 45 km downwind of the wind farm. According to the simulation, this wake was long enough to reach the wind farm Butendiek located 50 km downwind of Amrumbank West. In the spanwise direction, the wake has dimensions of approximately 12 km, similar to the maximal width of the wind farms AM, MSO and NO. The width of the simulated wake decreases with increasing distance from the wind farms but not the observed wake. For example, 35 km downwind of the wind farm, the simulations show a narrowing wake compared to the first flight leg by approximately 5 %.

The model underestimates the wind speed upwind of the wind farm, consequently the wind speed downwind of the wind farm is expected to be lower in the simulations than the observed one. Indeed, the difference WRF (interpolated onto the flight track) minus observation shows mostly negative values, indicating that the WRF simulation underpredicts the wind speed in and outside of the wake (Figure 4d and Figure 7e). The deviation outside of the wake is greater than inside the wake. Inside the wake, the model underpredicts the wind speed by up to $-0.6\,\mathrm{m\,s^{-1}}$ whereas outside of the wake, the deviations are more than three times larger by up to $-1.7\,\mathrm{m\,s^{-1}}$. This is especially true for the wind field located on the western side of the wake. A strong gradient in the wind field is present between the wake and the undisturbed flow in the observations. This gradient

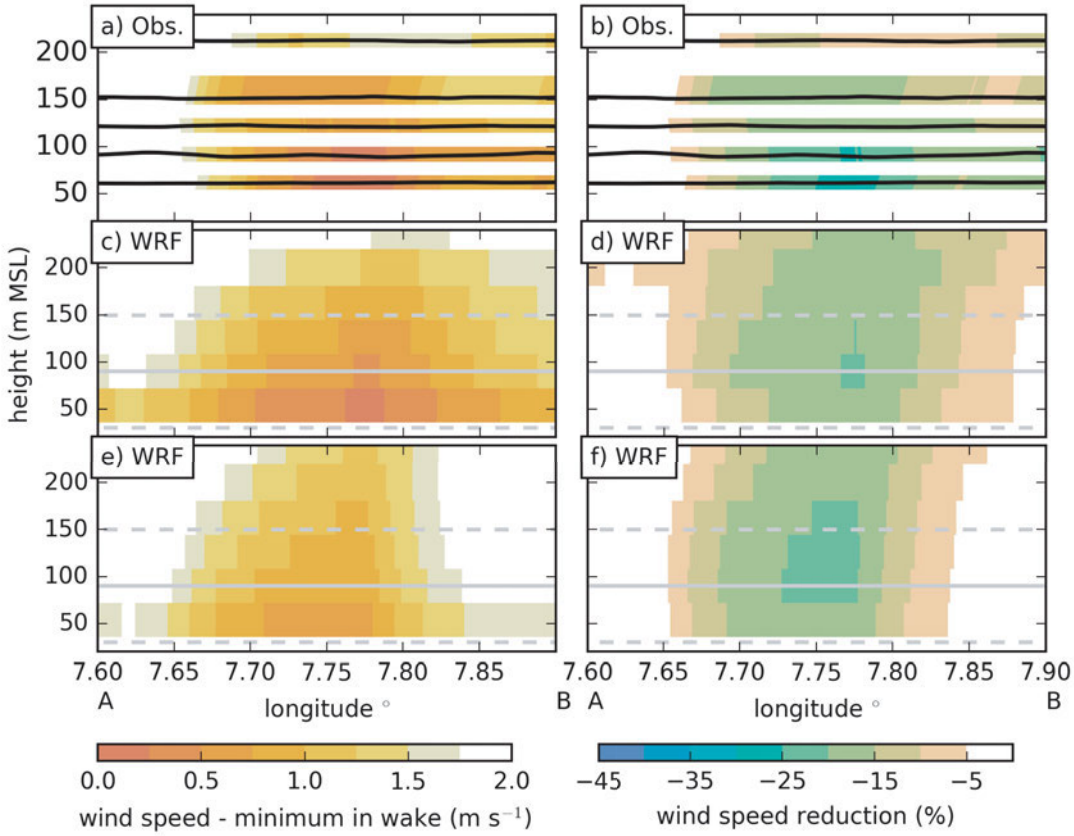

Figure 8: A comparison between aircraft measurements (a–b) and WRF simulation (c–d 1000 UTC and e–f 1100 UTC) along the vertical cross section perpendicular to the main flow, 5 km downwind of the wind farms as indicated in Figure 7a). Panels (a), (c) and (e) show the wind speed difference between wind speed minimum within the wake and surrounding wind speed in colored contours, indicating a measure of wind deficit recovery (as larger the difference as faster the wind speed recovers). Panels (b), (d) and (f) show the relative wind speed reduction in percent using colored contours. In the observational panels (a) and (b) the flight tracks are denoted as black thick lines. In the simulation panels (c–f), the hub height is indicated by a grey solid line, the upper and lower end of the rotor area is made visible by the grey dashed line. The simulation results (c–f) are shown by using a pixel plot to highlight the resolution of the model.

is not resolved in the simulations, consequently a large error is observed on the western edge of the far field.

Within the wake, the errors are much lower: for example, at the first flight leg downwind of the wind farm, the simulated wake has a wind speed of 6.0 m s^{-1}, whereas 6.5 to 7.0 m s^{-1} were observed. Corresponding to this result, the difference WRF – observation (Figure 7f) is between −0.8 m s^{-1} to −0.2 m s^{-1} within the wake region. Further downwind, at the second and the third flight leg, the error decreases within the wake region and errors of around −0.2 m s^{-1} and 0.2 m s^{-1} are observed.

From the third flight leg downwind, the wake is shifted more to the east in the model compared to the flight measurements. Therefore, the model overestimates the wind speed within the observed wake region by up to 0.5 m s^{-1} and underestimates the wind speed outside of the observed wake region by up to 0.4 m s^{-1}.

4.3.2 Vertical extent of the wake

Here we examine the vertical extent of the wind speed deficit 5 km downwind of the wind farms. The research aircraft flew at five different heights 5 km downwind of the wind farms to capture the vertical wind speed deficit as explained in Section 2.2. We focus on the actual ability of the model to simulate the vertical dimensions of the wake. Therefore, we show in Figure 8a,c,e) the difference between wind speed minimum within the wake and the surrounding wind speed. For simplicity we refer to this difference as *wind deficit recovery*.

We also show the wind speed reduction in percent. For the simulation the wind speed reduction was calculated by comparison of a simulation without and with wind farms. To estimate an observed wind speed reduction, we assume an undisturbed wind speed of 8.5 m s^{-1}, corresponding to the wind speed on the western side of the wake (Figure 7d). However, it has to be kept in mind that a wind speed gradient extended from east to west. Therefore, the wind speed reduction values on the eastern edge of the wake are biased. Further, wind speed is most of the time increasing with height. Hence, the observed wind reduction values at 60 m and 220 m should be considered carefully.

The measurements and the model show both a wind speed reduction well above the rotor area (Figure 8). The

model overestimates the width of the wake at the western flank of the wake at 1000 UTC (Figure 8c). This error is rooted in the stronger horizontal wind speed gradient in the observations than in the simulations (Figure 7).

The minimum in the observed wake is more pronounced in the observations than in the simulations (Figure 8). Within the center of the wake, the wind deficit recovery has values between 0 and 0.5 m s^{-1} between 60 m and 90 m in the observations, compared to values of over 0.5 m s^{-1} in the simulations (Figure 8a,c,e). The wake recovers faster in vertical directions in the simulations at 1000 UTC (Figure 8c). However, at 1100 UTC the simulation shows a wake exceeding the vertical dimensions of the observed one (Figure 8e).

When we show the wind speed deficit in percent, the model seems to overestimate the vertical extent of the wake. Further, the wake center is located 20 m higher than in the measurements and underestimated by 5 percent. In contrast, the horizontal gradient of the relative wind reduction matches the observed one at the western flank of the wake, which is not the case for the wind deficit recovery.

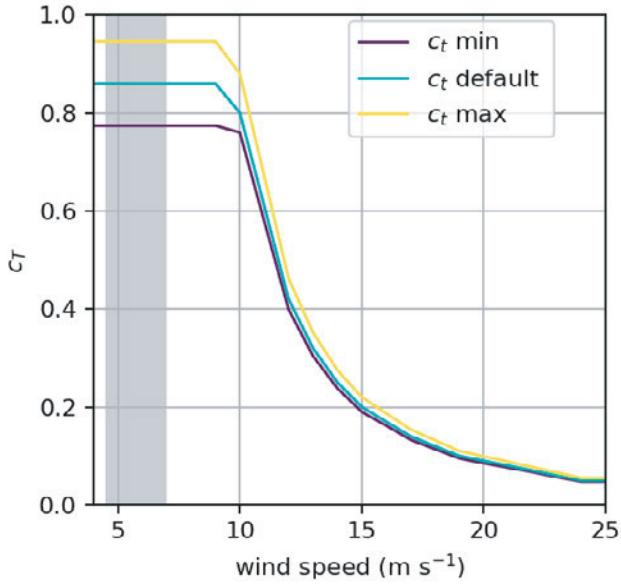

Figure 9: Variation of the thrust coefficient c_T. During the field campaign the upwind wind speed at hub height was between 4.5 m s^{-1} and 7.4 m s^{-1} in the model simulations, this wind speed interval is shaded grey. In yellow and purple the minimum and maximum thrust coefficients are plotted, respectively. In cyan the thrust coefficient of the control run is shown.

5 Sensitivity experiment

In this section, we assess the uncertainty of the simulations regarding the estimated thrust and power coefficients. The difference between the power and the thrust coefficients alone determines the fraction of energy that is extracted from the mean flow to turbulent kinetic energy by the wind farm parameterization (see equation 12 in Fitch et al., 2012). Consequently, varying only one coefficient within a large enough interval should cover the uncertainty that stems from the estimated wind farm coefficients.

We conducted two sensitivity studies, by increasing and decreasing the thrust coefficient with respect to the thrust coefficient of the control simulation by ten percent, resulting in the thrust coefficients curves, denoted as $c_{T\,max}$ and $c_{T\,min}$ in Figure 9. The WRF model simulates for the observational period, upwind of the wind farms, wind speeds within the interval of 4.5 m s^{-1} and 7.0 m s^{-1}. Therefore, the uncertainty of the power and thrust coefficient is restricted to this wind speed interval (see grey marked wind speed interval in Figure 9). The empirical thrust coefficient function of Magnusson (1999) gives for this wind speed interval, a thrust coefficient in the order of 0.8 and 0.85, whereby Jiménez et al. (2007) assume a thrust coefficient of 0.75 for winds speeds within 7–10 m s^{-1}. Therefore, our thrust coefficient interval from 0.776 to 0.946 should encompass the uncertainty.

The results of the sensitivity studies are shown in Figure 10. To emphasis the effect of the varying thrust coefficient we show the difference between simulation without and with a wind farm parameterization (i.e. simulation with wind farms − simulation without wind farms). The difference was calculated with hourly averaged data to achieve a clear signal of the wind farm parameterization.

All three simulations show similar results. All simulated wakes extend beyond 45 km downwind of the wind farms. Additionally, they do not differ much in their intensity. They all show a maximum wind speed reduction of −1.4 m s^{-1}. As expected the simulation with the highest thrust coefficient $c_{T\,max}$ shows the most pronounced wind speed reduction of -1.4 m s^{-1}. However, the wind speed reduction differences in the simulations are not bigger than 0.2 m s^{-1}. From 30–45 km downwind, all simulations show a wind speed reduction of 5 % (or −0.4 m s^{-1}).

All three simulations show an acceleration at the flanks of the wakes, whereby the acceleration at the left flank is more defined than on the right side looking into flow direction. Further, the acceleration is more pronounced for a higher thrust coefficient indicating that the acceleration is rooted in the mass continuity. The simulation $c_{T\,min}$ shows only accelerations on the left flank with speed ups of maximum 0.4 m s^{-1}, increasing to a defined streak with an increasing thrust coefficient. On the right flank of the wake, an acceleration is also visible, but the acceleration is below 0.2 m s^{-1} (i.e. below 5 %) and twice as broad as the wake.

The streak of wind speed reduction shown in all three simulations in the south west is caused by the wind farm Godewind. This wake was not measured by the aircraft and is therefore not discussed in this study. However, the wind farm was considered in our simulations so as to be accommodate of any wake interactions.

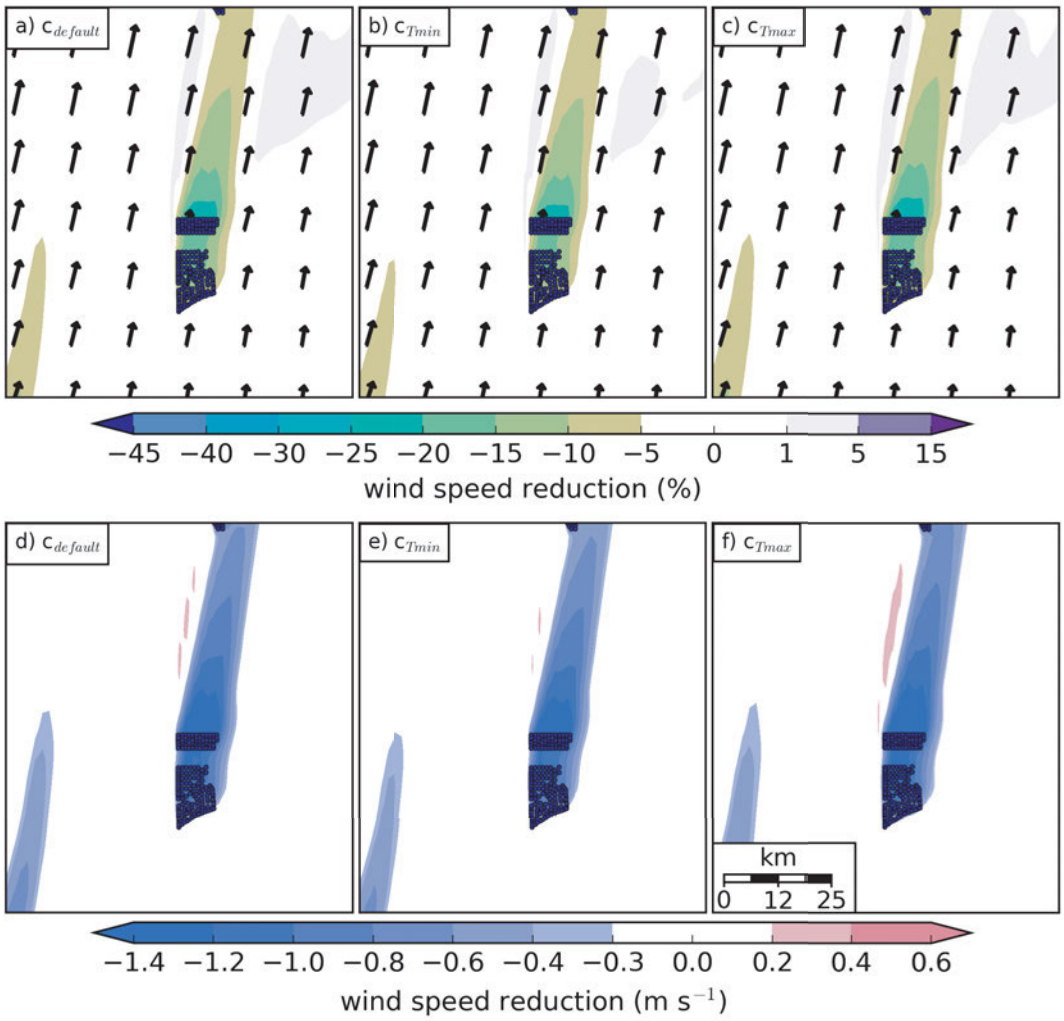

Figure 10: The sensitivity of the wind farm parameterization with respect to the varying thrust coefficients shown in Figure 9. Panel (a), (b) and (c) show the relative wind speed deficit and speed up (colored contours) compared to a simulation without wind farms at 0900 UTC 10 September 2016. Panel (d)–(f) show the corresponding total change in wind speed in colored contours whereby blue and red contours indicate a wind speed deficit and speed up, respectively. All data used for this figure was averaged over one hour.

6 Discussion

The WRF model with the wind farm parameterization of Fitch et al. (2012) simulated the wake generated by the wind farms AW, MSO and NO reasonably well. The length and width of the wake were simulated correctly, although the upwind wind speed was too low.

We assert that this wind speed deviation between model and observation is rooted in the neutrally stratified lower atmosphere (see Figure 4) in the simulation. A more stable-stratified atmosphere would result in a more pronounced low-level jet and, hence, a vertical wind profile with higher wind speeds at hub height.

This neutrally stratified atmosphere is in turn caused by the overestimated cold air advection close to the coast (at FINO1). As we have shown (Figure 4) the vertical potential temperature profile obtained by the aircraft was similar to the sounding of the island Norderney measured eight hours earlier at 0000 UTC, located approx. 100 km upwind of the wind farm Nordsee Ost. Therefore, the upwind potential temperature profile was characterized by the nocturnal cooling over the land. The too-cold simulated upwind vertical potential temperature profile emphasizes that the WRF model overestimates the nocturnal cooling over land. Consequently, too cold air masses are advected over the North Sea in the model. This in turn causes a delayed warming of the atmosphere close to the coast and explains the models temperature deviation at FINO1. Hence, we suggest that the wrong stratification at FINO1 is rooted in the overestimated night time cooling over land.

This deviation between the model and observed stratification at FINO1 raises the question whether the simulated wake is realistic. As the model has only difficulties capturing the stratification of the marine boundary layer close to the coast and not further downwind (i.e. the WRF model performed well at FINO3, see Section 4.1) we assert that the modeled wake is realistic.

An underestimation of the wind speed in the WRF model was already reported in previous works. Hasager et al. (2015) compared wakes of wind speeds upwind and downwind of Horns Rev 1 from SAR images and WRF results. WRF captured the wind speed distribution around Horns Rev 1, but also underestimated the wind speed in the undisturbed flow and, hence, also within in the wake region. They noticed a deviation between WRF and SAR images outside of the wake in the order of 1.5 m s^{-1}, whereby within the wake they reported a deviation below 1 m s^{-1}. They compared 10 m winds retrieved from the satellite images against simulated winds at 10 m above MSL. These results correspond to our observations where we have deviations of 1.7 m s^{-1} outside of the wake and 0.5 m s^{-1} inside the wake. Also Hahmann et al. (2015) showed that regardless of the boundary conditions, WRF underestimates the wind speed at FINO1 for a simulation covering the year 2010. That indicates that the most potential for improvement of forecasting offshore wakes for this specific case is rooted in a better representation of the marine atmospheric boundary layer and not in the wind farm parameterization. This finding agrees with the result of Lee and Lundquist (2017), who also found that the main error is rooted in the background flow and not in the wind farm parameterization.

Deviations between observation and simulations that are introduced due to estimated thrust- and power coefficients are minor compared to the deviations caused by the background errors. We demonstrated this insensitivity by varying the thrust coefficient by ±10 % and the wind speed deficit in the wake increased (decreased) by 0.2 m s^{-1}. Compared to a background deviation of up to 1.9 m s^{-1} this is a rather small source of error.

Our results showed that forecasting wind direction correctly is important for realistic power predictions for offshore sites. This is in contrast to the finding of Lee and Lundquist (2017) for an onshore site. They showed that the forecasted wind direction did not significantly influence the quality of the wind power forecast. This can be explained by the rather long wakes possible over the North Sea (as in this case study) compared to onshore sites. For example, the observed wake reached a length of up to 45 km. That means that a deviation between observed and simulated wind direction of 5 degrees leads to a 5 km displacement of the wake. These 5 km can be crucial as they can decide whether a downwind wind farm is affected by a wake or not.

Not all features in the observed wake can be resolved by a mesoscale model. For example, the strong gradient at the western flank in the observed wake (Figure 7) is a detail that can not be resolved in a mesoscale simulation, because the grid size is too large. According to Skamarock (2004) physical solutions only exist for processes that have the size seven times the grid spacing of the model. Consequently, a decrease in wind speed over the distance of 3 km can not be resolved by a mesoscale model. For such purposes RANS, URANS, or large-eddy-simulations need to be applied.

7 Conclusion

The wind farm parameterization of Fitch et al. (2012) has been evaluated for a cluster of offshore wind farms based on aircraft measurements. The aim was to test the performance of a mesoscale wind farm parameterization for a real case simulation. Therefore, it was also necessary to evaluate the model's ability to simulate the boundary layer upwind of the wind farms as the wake highly depends on the configuration of the upwind flow. These are the key findings:

- The deviation in the background flow dominates the deviation of observed and simulated wake. A large scale southerly forcing advected continental air masses over the North Sea. These air masses were characterized by a nocturnal inversion at the beginning and by a mixed layer during the second half of our observation. Consequently, the stratification of the marine boundary layer was influenced by the boundary layer of the land upwind. The advection of the nocturnal inversion caused a weakly stratified marine boundary layer close to the coast as the advected air masses were colder than the SST. Later, air warmer than the SST was advected and a stable marine atmospheric boundary layer developed. The mesoscale Weather Research and Forecasting Model had problems resolving the transition of the marine boundary layer from stably to weakly stratified upwind of the wind farms. As the wind profile depends on the stability, the upwind wind speed was underestimated (i.e. up to 1.9 m s^{-1}).
- The wind farm parameterization simulates the spatial dimensions of the wake well. Despite the fact that we have a deviation in the upwind flow at the transition area between land to open sea, the model represents the atmosphere in the far wake region – 150 km away from the coast – well. Therefore, the parameterization represents the wind deficit measurable 45 km downwind of the wind farms. Additionally, the parameterization can represent the horizontal and vertical expansion of the wake 5 km downwind of the wind farms. In the observation and the simulations, a wind speed deficit is still clearly visible approximately 70 m above the upper end of the rotor area. However, the model has the tendency to overestimate the vertical dimensions of the wake due to a too unstable boundary layer in the model. However, although the spatial dimensions agree with the observed ones, the absolute wind speed values disagree with the measurements. As the model underestimates the upwind wind speed, the wind speed within the wake is also lower than in the observations.
- We further showed that deviations that are introduced due to uncertainties in the thrust and power coefficients only cause small deviations compared to the aforementioned deviation in the upwind flow.

These results indicate that the performance of wind farm parameterizations is for stably stratified atmospheres limited by the performance of the driving mesoscale model. As many existing and planned wind farms are within 100 km the coast, boundary layer parameterizations that better represent the transition between land and open sea are necessary.

Acknowledgments

The WIPAFF project is funded by the German Federal Ministry of Economic Affairs and Energy (grant number: FKZ 0325783) on basis of a decision by the German Bundestag. We acknowledge support by Deutsche Forschungsgemeinschaft and Open Access Publishing Fund of Karlsruhe Institute of Technology. JKL's efforts were supported by the National Science Foundation under grant BCS-1413980 (Coupled Human Natural Systems). GRACE funded the research stay at the University of Boulder of SKS. Further, we want to thank Alexander Gohm for his advice considering the simulations. The calculations were performed on the Kea cluster of KIT/IMK-IFU. This cluster was gratefully managed by Dominikus Heinzeller. We thank Richard Fruehmann and Andreas Mark for explaining the uncertainties in the temperature measurements of FINO1 and FINO3.

References

Abkar, M., F. Porté-Agel, 2015: A new wind-farm parameterization for large-scale atmospheric models. – J. Renew. Sustain. Energy **7**, 013121, DOI: 10.1063/1.4907600.

Baidya Roy, S., J.J. Traiteur, 2010: Impacts of wind farms on surface air temperatures. – PNAS **107**, 17899–17904, DOI: 10.1073/pnas.1000493107.

Bilgili, M., A. Yasar, E. Simsek, 2011: Offshore wind power development in Europe and its comparison with onshore counterpart. – J. Renew. Sustain. Energy Rev. **15**, 905–915, DOI: 10.1016/j.rser.2010.11.006.

Blahak, U., B. Goretzki, J. Meis, 2010: A simple parameterization of drag forces induced by large wind farms for numerical weather prediction models. – In: Proceedings of the European Wind Energy Conference & Exhibition.

Bodini, N., D. Zardi, J.K. Lundquist, 2017: Three-dimensional structure of wind turbine wakes as measured by scanning lidar. – Atmos. Meas. Tech. **10**, 2881, DOI: 10.5194/amt-10-2881-2017.

Brümmer, B., G. Müller, D. Schröder, A. Kirchgässner, J. Launiainen, T. Vihma, 2003: The eight baltimos field experiments 1998–2001 over the baltic sea. – International BALTEX Secretariat, Publication Series **138**.

Bundesnetzagentur, 2017: Anlagenregister. – Available online at https://www.bundesnetzagentur.de/DE/Sachgebiete/ElektrizitaetundGas/Unternehmen_Institutionen/ErneuerbareEnergien/ZahlenDatenInformationen/EEG_Registerdaten/EEG_RegDaten_FoerdSaetze.html, accessed October 9, 2018.

Calaf, M., C. Meneveau, J. Meyers, 2010: Large eddy simulation study of fully developed wind-turbine array boundary layers. – Phys. Fluids **22**, 015110, DOI: 10.1063/1.3291077.

Calaf, M., M.B. Parlange, C. Meneveau, 2011: Large eddy simulation study of scalar transport in fully developed wind-turbine array boundary layers. – Phys. Fluids **23**, 126603, DOI: 10.1063/1.3663376.

Chatelain, P., S. Backaert, G. Winckelmans, S. Kern, 2013: Large eddy simulation of wind turbine wakes. – Flow Turbulence Combust. **91**, 587–605, DOI: 10.1007/s10494-013-9474-8.

Chatterjee, F., D. Allaerts, U. Blahak, J. Meyers, N. van Lipzig, 2016: Evaluation of a wind-farm parametrization in a regional climate model using large eddy simulations. – Quart. J. Roy. Meteor. Soc. **142**, 3152–3161, DOI: 10.1002/qj.2896.

Chen, F., J. Dudhia, 2001: Coupling an Advanced Land Surface-Hydrology Model with the Penn State-NCAR0 MM5 Modeling System. Part I: Model Implementation and Sensitivity. – Mon. Wea. Rev. **129**, 569–585, DOI: 10.1175/1520-0493(2001)129<0569:CAALSH>2.0.CO;2.

Christiansen, M.B., C.B. Hasager, 2005: Wake effects of large offshore wind farms identified from satellite SAR. – Remote Sens. Env. **98**, 251–268, DOI: 10.1016/j.rse.2005.07.009.

Corsmeier, U., R. Hankers, A. Wieser, 2001: Airborne turbulence measurements in the lower troposphere onboard the research aircraft Dornier 128-6, D-IBUF. – Meteorol. Z. **10**, 315–329, DOI: 10.1127/0941-2948/2001/0010-0315.

Djath, B., J. Schulz-Stellenfleth, B. Cañadillas, 2018: Impact of atmospheric stability on X-band and C-band synthetic aperture radar imagery of offshore windpark wakes. – J. Renew. Sustain. Energy **10**, 043301.

Dörenkämper, M., M. Optis, A. Monahan, G. Steinfeld, 2015: On the Offshore Advection of Boundary-Layer Structures and the Influence on Offshore Wind Conditions. – Boundary-Layer Meteorol. **155**, 459–482, DOI: 10.1007/s10546-015-0008-x.

Emeis, S., 2010: A simple analytical wind park model considering atmospheric stability. – Wind Energy **13**, 459–469, DOI: 10.1002/we.367.

Emeis, S., S. Siedersleben, A. Lampert, A. Platis, J. Bange, B. Djath, J. Schulz-Stellenfleth, T. Neumann, 2016: Exploring the wakes of large offshore wind farms. – J. Phys. **753**, 092014.

Fitch, A.C., 2015: Notes on using the mesoscale wind farm parameterization of Fitch et al. (2012) in WRF. – Wind Energy **19**, 1757–1758, DOI: 10.1002/we.1945.

Fitch, A.C., J.B. Olson, J.K. Lundquist, J. Dudhia, A.K. Gupta, J. Michalakes, I. Barstad, 2012: Local and Mesoscale Impacts of Wind Farms as Parameterized in a Mesoscale NWP Model. – Mon. Wea. Rev. **140**, 3017–3038, DOI: 10.1175/MWR-D-11-00352.1.

Fitch, A.C., J.K. Lundquist, J.B. Olson, 2013a: Mesoscale influences of wind farms throughout a diurnal cycle. – Mon. Wea. Rev. **141**, 2173–2198, DOI: 10.1175/MWR-D-12-00185.1.

Fitch, A.C., J.B. Olson, J.K. Lundquist, 2013b: Parameterization of Wind Farms in Climate Models. – J. Climate **26**, 6439–6458, DOI: 10.1175/JCLI-D-12-00376.1.

Frandsen, S., R. Barthelmie, S. Pryor, O. Rathmann, S. Larsen, J. Højstrup, M. Thøgersen, 2006: Analytical modelling of wind speed deficit in large offshore wind farms. – Wind Energy **9**, 39–53, DOI: 10.1002/we.189.

Friehe, C., W. Shaw, D. Rogers, K. Davidson, W. Large, S. Stage, G. Crescenti, S. Khalsa, G. Greenhut, F. Li, 1991: Air-sea fluxes and surface layer turbulence around a sea surface temperature front. – J. Geophys. Res. **96**, 8593–8609, DOI: 10.1029/90JC02062.

Fruehmann, R., 2016: Relative calibration process for long term thermal stratification measurements in the lower atmospheric boundary layer. – DEWI Magazin **48**, pub-

lished online. https://www.dewi.de/dewi_res/fileadmin/pdf/publications/Magazin_48/DEWI_Magazin_48_Digital.pdf.

Hahmann, A.N., C.L. Vincent, A. Peña, J. Lange, C.B. Hasager, 2015: Wind climate estimation using WRF model output: method and model sensitivities over the sea. – Int. J. Climatol. **35**, 3422–3439, DOI: 10.1002/joc.4217.

Hasager, C.B., P. Vincent, J. Badger, M. Badger, A. Di Bella, A. Peña, R. Husson, P.J. Volker, 2015: Using Satellite SAR to Characterize the Wind Flow Around Offshore Wind Farms. – Energies **8**, 5413–5439, DOI: 10.3390/en8065413.

Iacono, M.J., J.S. Delamere, E.J. Mlawer, M.W. Shephard, S.A. Clough, W.D. Collins, 2008: Radiative forcing by long-lived greenhouse gases: Calculations with the AER radiative transfer models. – J. Geophys. Res. **113**, DOI: 10.1029/2008JD009944.

Ivanova, L.A., E.D. Nadyozhina, 2000: Numerical simulation of wind farm influence on wind flow. – Wind Engineering **24**, 257–269, DOI: 10.1260/0309524001495620.

Jacobson, M.Z., C.L. Archer, 2012: Saturation wind power potential and its implications for wind energy. – PNAS **109**, 15679–15684, DOI: 10.1073/pnas.1208993109.

Jiménez, A., A. Crespo, E. Migoya, J. Garcia, 2007: Advances in large-eddy simulation of a wind turbine wake. – J. Phys. **75**, 012041.

Jiménez, P.A., J. Navarro, A.M. Palomares, J. Dudhia, 2015: Mesoscale modeling of offshore wind turbine wakes at the wind farm resolving scale: a composite-based analysis with the Weather Research and Forecasting model over Horns Rev. – Wind Energy **18**, 559–566, DOI: 10.1002/we.1708.

Kaffine, D.T., C.M. Worley, 2010: The windy commons? – Env. Resource Econ. **47**, 151–172, DOI: 10.1007/s10640-010-9369-2.

Kain, J.S., 2004: The Kain–Fritsch Convective Parameterization: An Update. – J. Appl. Meteor. Climatol. **43**, 170–181, DOI: 10.1175/1520-0450(2004)043<0170:TKCPAU>2.0.CO;2.

Keith, D.W., J.F. DeCarolis, D.C. Denkenberger, D.H. Lenschow, S.L. Malyshev, S. Pacala, P.J. Rasch, 2004: The influence of large-scale wind power on global climate. – PNAS **101**, 16115–16120, DOI: 10.1073/pnas.0406930101.

Lee, J.C.Y., J.K. Lundquist, 2017: Evaluation of the wind farm parameterization in the Weather Research and Forecasting model (version 3.8.1) with meteorological and turbine power data. – Geosci. Model Dev. **10**, 4057–4079, DOI: 10.5194/gmd-2017-128.

Lim, K.S.S., S.Y. Hong, 2010: Development of an effective double-moment cloud microphysics scheme with prognostic cloud condensation nuclei (CCN) for weather and climate models. – Mon. Wea. Rev. **138**, 1587–1612, DOI: 10.1175/2009MWR2968.1.

Magnusson, M., 1999: Near-wake behaviour of wind turbines. – J. Wind Engineer. Indust. Aerodyn. **80**, 147–167, DOI: 10.1016/S0167-6105(98)00125-1.

Mann, J., D.H. Lenschow, 1994: Errors in airborne flux measurements. – J. Geophys. Res. **99**, 14519–14526.

Nakanishi, M., H. Niino, 2004: An improved Mellor–Yamada level-3 model with condensation physics: Its design and verification. – Boundary-Layer Meteorol. **112**, 1–31, DOI: 10.1023/B:BOUN.0000020164.04146.98.

Neumann, T., K. Nolopp, K. Herklotz, 2004: First operating experience with the FINO1 research platform in the North Sea. – DEWI Magazin **24**, 27–32.

Nygaard, N.G., 2014: Wakes in very large wind farms and the effect of neighbouring wind farms. – J. Phys. **524**, 012162.

Nygaard, N.G., S.D. Hansen, 2016: Wake effects between two neighbouring wind farms. – J. Phys. **753**, 032020.

Platis, A., S.K. Siedersleben, J. Bange, A. Lampert, K. Bärfuss, R. Hankers, B. Cañadillas, R. Foreman, J. Schulz-Stellenfleth, B. Djath, T. Neumann, S. Emeis, 2018: First in situ evidence of wakes in the far field behind offshore wind farms. – Sci. Rep. **8**, 2163, DOI: 10.1038/s41598-018-20389-y.

Porté-Agel, F., Y.T. Wu, H. Lu, R.J. Conzemius, 2011: Large-eddy simulation of atmospheric boundary layer flow through wind turbines and wind farms. – J. Wind Eng. Ind. Aerodyn. **99**, 154–168, DOI: 10.1016/j.jweia.2011.01.011.

Shimada, S., T. Ohsawa, T. Kogaki, G. Steinfeld, D. Heinemann, 2015: Effects of sea surface temperature accuracy on offshore wind resource assessment using a mesoscale model. – Wind Energy **18**, 1839–1854.

Skamarock, W.C., 2004: Evaluating mesoscale NWP models using kinetic energy spectra. – Mon. Wea. Rev. **132**, 3019–3032, DOI: 10.1175/MWR2830.1.

Skamarock, W., J. Klemp, J. Dudhia, D. Gill, D. Barker, M. Duda, X. Huang, W. Wang, J. Powers, 2008: A description of the advanced research WRF version 3, NCAR. – Technical report, Mesoscale and Microscale Meteorology Division, National Center for Atmospheric Research, Boulder, Colorado, USA, available online at www2.mmm.ucar.edu/wrf/users/docs.

Smedman, A.S., U. Högström, H. Bergström, 1996: Low level jets – a decisive factor for off-shore wind energy siting in the Baltic Sea. – Wind Engineer. **20**, 137–147.

Smedman, A.S., H. Bergström, B. Grisogono, 1997: Evolution of stable internal boundary layers over a cold sea. – J. Phys. **102**, 1091–1099, DOI: 10.1029/96JC02782.

Svensson, N., H. Bergström, E. Sahlée, A. Rutgersson, 2016: Stable atmospheric conditions over the Baltic Sea: model evaluation and climatology. – Boreal Env. Res. **21**, 387–404.

Vanderwende, B.J., B. Kosović, J.K. Lundquist, J.D. Mirocha, 2016: Simulating effects of a wind-turbine array using LES and RANS. – J. Adv. Model. Earth Sys. **8**, 1376–1390, DOI: 10.1002/2016MS000652.

Volker, P., J. Badger, A.N. Hahmann, S. Ott, 2015: The Explicit Wake Parametrisation V1.0: a wind farm parametrisation in the mesoscale model WRF. – Geosci. Model Dev. **8**, 3715–3731, DOI: 10.5194/gmd-8-3715-2015.

WindEurope, 2016: Wind in power 2015 European statistics. – Available online at https://windeurope.org/wp-content/uploads/files/about-wind/statistics/EWEA-Annual-Statistics-2015.pdf, accessed October 9, 2018.

Wu, Y.T., F. Porté-Agel, 2015: Modeling turbine wakes and power losses within a wind farm using LES: An application to the Horns Rev offshore wind farm. – Renew. Energy **75**, 945–955, DOI: 10.1016/j.renene.2014.06.019.

Zhou, L., Y. Tian, S.B. Roy, C. Thorncroft, L.F. Bosart, Y. Hu, 2012: Impacts of wind farms on land surface temperature. – Nat. Clim. Chang. **2**, 539–543, DOI: 10.1038/NCLIMATE1505.